Possible multiple antimagnetic rotational bands in odd-A ^{103,105}Pd and ^{109}Cd nuclei*

Yu-Kun Pan(潘禹坤)   Ke-Yan Ma(马克岩)[†]   Jing-Bin Lu(陆景彬)[‡]

College of Physics, Jilin University, Changchun 130012, China

Abstract: The positive-parity signature partner bands in ^{103,105}Pd and ^{109}Cd nuclei are investigated using the classical particle-rotor model. Based on the systematic study of neighbouring nuclei, the signature partner bands of ^{105}Pd are assigned to the $\pi(g_{9/2}^{-4}) \otimes \nu(g_{7/2}h_{11/2}^2)$ configuration, and this assignment is also supported by the present calculations. Furthermore, the calculated $B(E2)$ values of such bands of ^{105}Pd reproduce the experimental values well and exhibit a decrease with increasing angular momentum, suggesting that these two bands may originate from antimagnetic rotation. Similar signature partner bands are also found in the neighboring ^{103}Pd and ^{109}Cd nuclei. The properties of both bands are in general agreement with the fingerprints of antimagnetic rotation, and thus the signature partner bands of ^{103}Pd and ^{109}Cd are suggested to be candidates for the multiple antimagnetic rotational bands of ^{105}Pd. In addition, the evolution of the two-shears-like mechanism for possible multiple antimagnetic rotational bands in ^{103,105}Pd and ^{109}Cd nuclei is examined by investigating the orientation of the angular momenta.

Keywords: signature partner band, multiple antimagnetic rotation, classical particle-rotor model

DOI: 10.1088/1674-1137/ac6dab

I. INTRODUCTION

The study of antimagnetic rotation (AMR) has been a popular topic in weakly deformed or nearly spherical nuclei in the past few years. AMR is a novel mechanism for the generation of high angular momentum states in atomic nuclei and was first proposed by Frauendorf [1, 2]. In this interpretation, the two angular momentum vectors of a pair of deformation-aligned protons (j_π) in reversed orbits are nearly perpendicular to the orientation of the total angular momentum vector of the valence neutrons (j_ν) at the band head. An increase in the total angular momentum is generated by the simultaneous closing of the two proton blades along the direction of the total angular momentum vector, while the direction of the total angular momentum stays unchanged. It behaves like the closing of a pair of shears; hence, this type of excitation is known as the 'two-shears-like mechanism'. This geometry preserves the symmetry of $R_z(\pi)$ [3] and causes the perpendicular components of the magnetic moments to precisely cancel each other out. In this scenario, the dipole transitions ($M1$) are not observed, and the energy levels in the bands are connected by weak $E2$ transitions, reflecting a nearly spherical core. Hence, the phenomenon of AMR is characterized by the appearance of weak $E2$ transitions, a decrease in the $B(E2)$ values with increasing spin, and a large $\Im^{(2)}/B(E2)$ ratio [1].

Experimentally, the observed AMR bands mainly focus on the $A \approx 110$, 140 mass regions. Among them, firm experimental evidence of AMR arising from lifetime measurements has been reported in ^{105,106,107,108,109,110}Cd [4−12], ^{100,101,103,104}Pd [3, 13−18], and ^{142,143}Eu [19, 20]. Moreover, several candidate AMR bands have been suggested in ^{111}Cd [9], ^{102}Pd [17], ^{108,109,110,112,113}In [21−25], ^{102}Ru [26], ^{144}Dy [27], ^{127}Xe [28], and ^{58}Fe [29].

Theoretically, AMR has been discussed using simple geometry in the classical particle-rotor model (PRM) [10, 11, 30], the cranking shell model with the particle-number-conserving method [31−34], and the tilted axis cranking (TAC) model [35]. For the TAC model, many applications have been performed in the framework of the microscopic-macroscopic model [5, 6, 13], pairing plus quadrupole model [2, 36], and covariant density functional theory (CDFT) [37−41]. In particular, using the point coupling effective interaction [42], TAC-CDFT not only successfully describes AMR, but also numerous other phenomena, such as magnetic rotation [43−46], chiral rotation [47−49], and the nuclear rod shape [50]. It is worth

mentioning that for the famous chiral and magnetic rotation, the PRM has also achieved great success for the description of chiral doublet bands [51−54] and shear bands [55].

For most antimagnetic rotational nuclei, only one AMR band has been observed in a single nucleus. Is it possible for more than one antimagnetic rotational band to exist in a single nucleus, that is, multiple antimagnetic rotational bands? Such possibilities of multiple antimagnetic rotational band was recently demonstrated in [107]Cd [8]. Therefore, it is interesting to explore more examples of multiple AMR and examine their two-shears-like manifestations in other nuclei. For this purpose, the neighboring isotone [105]Pd and isotope [109]Cd seem to be good candidates and are discussed here within the classical PRM.

II. CLASSICAL PARTICLE-ROTOR MODEL

To describe the interplay between the motion of particles and the collective rotation, Bohr and Mottelson [56] proposed to consider only a few valence particles, which move more or less independently in the deformed well of the core, and to couple them to a collective rotor that represents the remaining particles. This is the famous PRM, where one generally divides the Hamiltonian into two parts: a phenomenological part H_{coll}, which describes the inert core, and an intrinsic part H_{intr}, which microscopically describes a valence particle or a whole subgroup of particles near the Fermi level [57]. As a quantum-mechanical model, the PRM has been successfully applied to investigate nuclear rotation [58−62]

Recently, numerical calculations within the framework of a geometric model were devised to study the competition between the shears mechanism and core rotation [10, 11, 27, 30, 63]. In this model, high-j neutrons and high-j proton holes are represented by classical angular momentum vectors (blades). The total energy is expressed as the sum of the rotational energy of the core and an effective interaction of the form $V_2P_2(\theta)$ between the blades (see Eq. (1a)), which is similar to the Hamiltonian of the PRM, and the total energy is solved in the classical limit by the requirement that, at each spin, the shears angle minimizes the energy. Hence, the geometric model mentioned above is also known as the classical PRM by Macchiavelli and Clark [30, 63].

The classical PRM, initially developed by Macchiavelli *et al.* for magnetic rotation [30, 64], was extended by Sugawara and Roy *et al.* for AMR bands [10, 11, 27]. During the last two decades, the characteristic properties of AMR bands have been reasonably described with the help of the classical PRM in many nuclei, such as [105,106,107,108,109,110,111]Cd [8−11], [100,101,104]Pd [3, 15, 16], and [127]Xe [28]. In this study, we address the AMR character of the positive-parity band in [105]Pd within the frame-

work of the classical PRM. In this model, the energy $E(I)$ is given by

$$
\begin{aligned}
E(I) &= \frac{R^2}{2\Im} + V_2P_2(\theta) \\
&= \frac{(\boldsymbol{I}-j_\pi-\boldsymbol{j}_\nu)^2}{2\Im} + \frac{V_{\pi\nu}}{2}\left(\frac{3\cos^2\theta-1}{2}\right) \\
&+ \frac{V_{\pi\nu}}{2}\left(\frac{3\cos^2(-\theta)-1}{2}\right) - \frac{V_{\pi\pi}}{n}\left(\frac{3\cos^22\theta-3}{2}\right).
\end{aligned}
\tag{1}
$$

In Eq. (1b), the first term represents the rotational contribution, and the rest of the terms are the shear contributions. The second and third terms represent the repulsive interaction between the neutron particles and proton holes. The fourth term signifies the proton-proton (hole-hole) attractive interaction. j_π and $\boldsymbol{j}_\nu$ represent the angular momentum vectors of protons and neutrons, respectively, and $V_{\pi\nu}$ and $V_{\pi\pi}$ are the interaction strengths. There is a scaling factor 'n' determined by the actual number of particle-hole pairs for a single-particle configuration. The angular momentum generated by the interplay between collective rotation and AMR can be calculated by minimizing the excitation energy as a function of shear angle, that is, $dE(I)/d\theta=0$

$$
I = aj + 2j\cos\theta + \frac{1.5\Im V_{\pi\nu}\cos\theta}{j} - \frac{6\Im V_{\pi\pi}\cos2\theta\cos\theta}{nj},
\tag{2}
$$

or

$$
I = I_{sh} + \Im\omega_{sh},
\tag{3}
$$

where $j = j_\pi$, $a = j_\nu/j_\pi$, I_{sh} is the sum of the first two terms of Eq. (2). $\Im\omega_{sh}$ represents the interplay between the shears mechanism and collective rotation and is represented by the last two terms of Eq. (2). The parameter ω_{sh} represents the frequency associated with the shears mechanism, which can be computed through $(dE_{sh}/d\theta)/(dI_{sh}/d\theta)$, and is given by

$$
\omega_{sh} = \frac{1.5V_{\pi\nu}\cos\theta}{j} - \frac{6V_{\pi\pi}\cos2\theta\cos\theta}{nj}.
\tag{4}
$$

It must be noted that the magnitude of $\Im$ determines the extent of the interplay involved in generating the angular momentum in this model. The value of $\Im$ can be estimated from the equation

$$
\Im\omega|_{(\theta=0°)} = I_{max} - I_{sh}^{max},
\tag{5}
$$

where I_{max} is the highest observed angular momentum

state, $I_{\text{sh}}^{\max}$ is generated through AMR due to complete alignment of the proton holes ($\theta = 0°$), and

$$\omega_{\text{sh}}|_{\theta=0°} = \left(\frac{1.5V_{\pi\nu}}{j}\right) - \left(\frac{6V_{\pi\pi}}{nj}\right). \qquad (6)$$

In case of an AMR-plus-rotation model, the rotational frequency ω is given by

$$\omega = \omega_{\text{rot}} - \omega_{\text{sh}}, \qquad (7)$$

where $\omega_{\text{rot}} = \dfrac{1}{2\mathfrak{J}_{\text{rot}}}(2I+1)$ is the core rotational frequency, and $\mathfrak{J}_{\text{rot}}$ is the core moment of inertia, whose value can be estimated from the slope of the $I(\omega)$ plot of the ground-state band (before neutron alignment). The details of this classical model are given in Refs. [10, 11]. Thus, all the parameters of the present model can be fixed either from experimental data or the systematics of the mass region.

III. DISCUSSION

In a previous study, multiple AMR was proposed for the first time in a pair of signature partner bands 5 and 6 of ^{107}Cd with the configuration $\pi(g_{9/2}^{-2})\otimes\nu(g_{7/2}h_{11/2}^2)$ [8]. In the present study, we find that similar structures labeled bands 1 and 2 are also observed in the neighboring isotone ^{105}Pd. To further study the characteristics of the bands in ^{105}Pd, a $I(\omega)$ plot of bands 1 and 2 in ^{105}Pd is shown in Fig. 1(a) and compared with bands 5 and 6 in ^{107}Cd [8], which are interpreted as a pair of antimagnetic rotational bands. In Fig. 1(a), bands 1 and 2 of ^{105}Pd exhibit sharp backbends with an increase in aligned angular momentum of approximately $8\hbar$ at frequency $\hbar\omega \sim 0.4$ MeV. The backbends are due to the alignment of two neutrons in the $h_{11/2}$ orbital, which is the lowest band crossing in this mass region. Furthermore, note that bands 1 and 2 of ^{105}Pd and bands 5 and 6 of ^{107}Cd exhibit similar behavior, including the frequencies of the observed alignments and the corresponding increases in spin, which indicates that the bands of ^{105}Pd are likely built on the similar intrinsic configuration $\pi(g_{9/2}^{-4})\otimes\nu(g_{7/2}h_{11/2}^2)$.

In Fig. 1(b), the $B(E2)$ values of bands 1 and 2 in ^{105}Pd taken from Ref. [65] are compared with the corresponding data for bands 5 and 6 in ^{107}Cd. It is easy to see that the $B(E2)$ values exhibit similar behaviors in bands 1 and 2 of ^{105}Pd as well as bands 5 and 6 of ^{107}Cd, which show decreasing $B(E2)$ values with increasing spin. These properties agree well with the experimental characteristics of AMR. Indeed, bands 5 and 6 in ^{107}Cd have been suggested to be antimagnetic rotational bands. Hence, both bands 1 and 2 of ^{105}Pd may have a common origin from AMR.
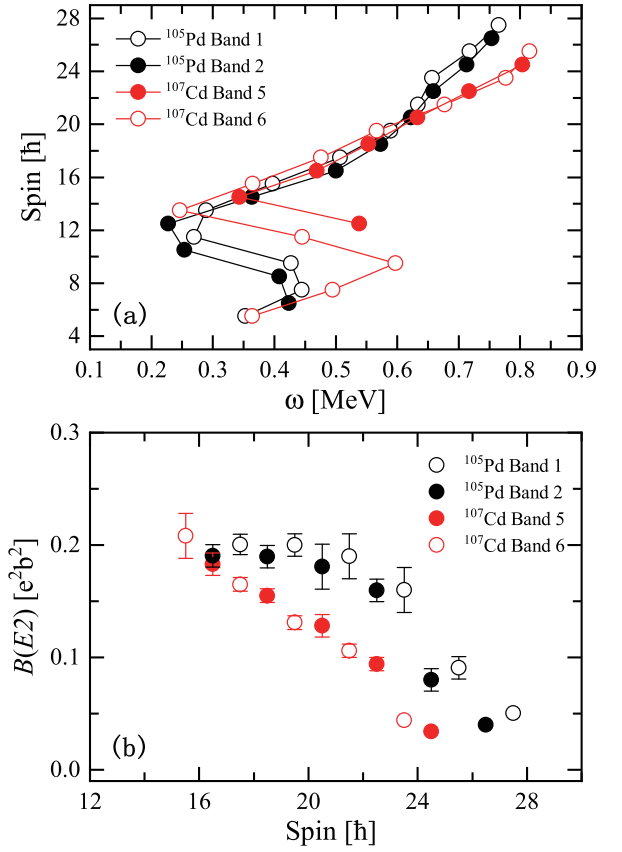

Fig. 1. (color online) Comparison of the spin angular momentum (a) and $B(E2)$ values (b) for bands 1 and 2 of ^{105}Pd and bands 5 and 6 of ^{107}Cd [8].

To further investigate the corresponding rotation mechanism of the positive-parity bands 1 and 2 in ^{105}Pd, the classical PRM is performed. In calculations, the corresponding single particle configuration for bands 1 and 2 of ^{105}Pd is $\pi(g_{9/2}^{-4})\otimes\nu(g_{7/2}h_{11/2}^2)$. This configuration has twelve proton-neutron combinations (n=12), and the interaction strengths $V_{\pi\nu}$ and $V_{\pi\pi}$ for both bands are expected to be 1.2 and 0.15 MeV, respectively, based on the systematic study of AMR bands in the $A \approx 110$ mass region [3, 11, 16].

In Fig. 2(a), the experimental angular momentum as functions of frequency for bands 1 and 2 are compared with the classical PRM calculations for the proposed configuration. As shown in Fig. 2(a), the calculations are in general agreement with the trend of the experimental angular momentum of bands 1 and 2, supporting the configuration assignment of the bands.

Typical characteristics of AMR include weak $E2$ transitions, reflecting the small deformation of the core, and a decreasing tendency of the reduced transition probability $B(E2)$ values with increasing spin, which results in large ratios of the dynamic moments of inertia $\mathfrak{J}^{(2)}$ to the $B(E2)$ values. Within the classical model description of the twin-shears mechanism for AMR, the $B(E2)$ values
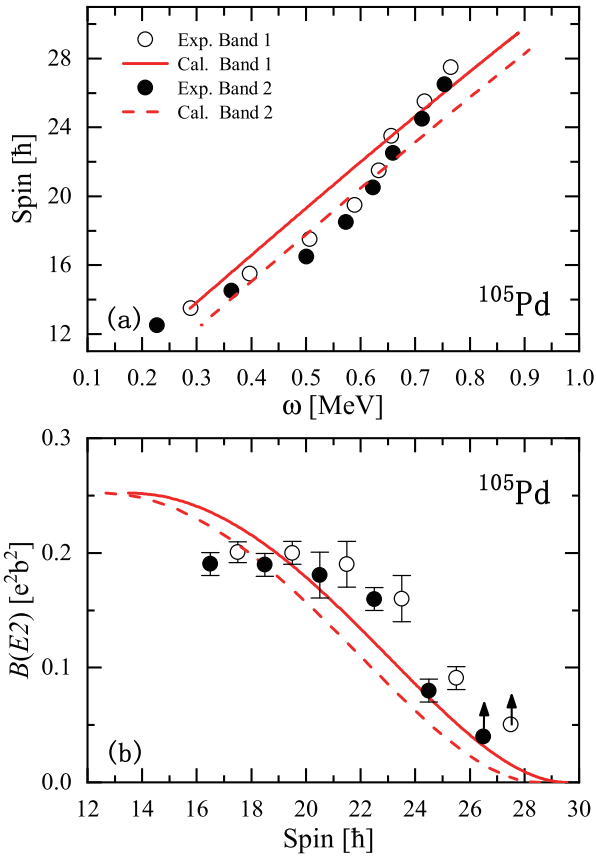
Fig. 2. (color online) Comparison of the measured I vs ω (a) and $B(E2)$ vs I (b) for bands 1 and 2 of ^{105}Pd. The red line represents the values calculated using the classical particle-rotor model. Values of $j_\pi = 6\hbar$, $\Im = 13.91\ \hbar^2\mathrm{MeV}^{-1}$, and $\Im_{\mathrm{rot}} = 18\ \hbar^2\mathrm{MeV}^{-1}$ have been used for both bands 1 and 2. The j_ν values of band 1 and 2 are $13.5\hbar$ and $12.5\hbar$, respectively.

can be written as

$$B(E2) = \frac{15}{32\pi}(eQ_{\mathrm{eff}})^2 \sin^4\theta. \qquad (8)$$

The $B(E2)$ values have been calculated using Eq. (8) for $eQ_{\mathrm{eff}} = 1.3$ eb [16], where θ and the total angular momentum are related by Eq. (2). The calculated $B(E2)$ values are shown by the red lines in Fig. 2(b). It is interesting to note that the calculated $B(E2)$ values of both bands 1 and 2 in ^{105}Pd exhibit a monotonically decreasing behaviour with increasing angular momentum, which agrees well with the experimentally obtained values taken from Ref. [65]. Moreover, the values of $\Im^{(2)}/B(E2)$ are also calculated, and it is found that the values are substantial ($> 100\ \hbar^2\mathrm{MeV}^{-1}(\mathrm{eb})^{-2}$). These results are consistent with the characteristics of AMR.

It is worth noting that the shears angle (θ) is the only variable in the present model, and every angular momentum state corresponds to a unique θ, which is determined from Eq. (2). To examine the two-shears-like mech-

anism for the candidate AMR bands in ^{105}Pd, a pictorial representation of the generation of the angular momentum by the closing of the twin-shears structure over the observed spin range in ^{105}Pd is shown in Fig. 3. For the signature partner bands 1 and 2 of ^{105}Pd with the $\pi(g_{9/2}^{-4}) \otimes \nu(g_{7/2}h_{11/2}^2)$ configuration, the angular momentum vectors $\boldsymbol{j}_\pi$ are almost perpendicular to $\boldsymbol{j}_\nu$ at the bandhead. Together with the valence particle angular momentum vectors $\boldsymbol{j}_\nu$, they form the blades of the two shears. With increasing rotational frequency, the gradual alignment of the proton hole angular momentum vectors toward the particle vectors generates a higher angular momentum. Because the direction of $\boldsymbol{I}_{\mathrm{sh}}$ remains unchanged, the two shears simultaneously close by moving one blade toward the other. In such a way, the two-shears-like mechanism in ^{105}Pd is clearly demonstrated in Fig. 3.

Furthermore, positive-parity signature partner bands with the same neutron configuration have also been found in neighboring ^{103}Pd and ^{109}Cd nuclei [66, 67]. As shown in Figs. 4(a) and (b), the $I(\omega)$ plot for the positive-parity signature partner bands of ^{103}Pd and ^{109}Cd is calculated using the classical PRM and compared with the experimental angular momentum. The calculated values are plotted as red lines in Figs. 4(a) and (b) for $V_{\pi\nu} = 1.2$ MeV and $V_{\pi\pi} = 0.15$ MeV. It is evident from the figures that the calculations are in general agreement with the trend of experimental angular momentum for the signature partner bands, which further supports the previous configuration assignment.

The calculated $B(E2)$ values and $\Im^{(2)}/B(E2)$ ratios are also shown as functions of the rotational frequency in the present calculations for the assigned configurations in

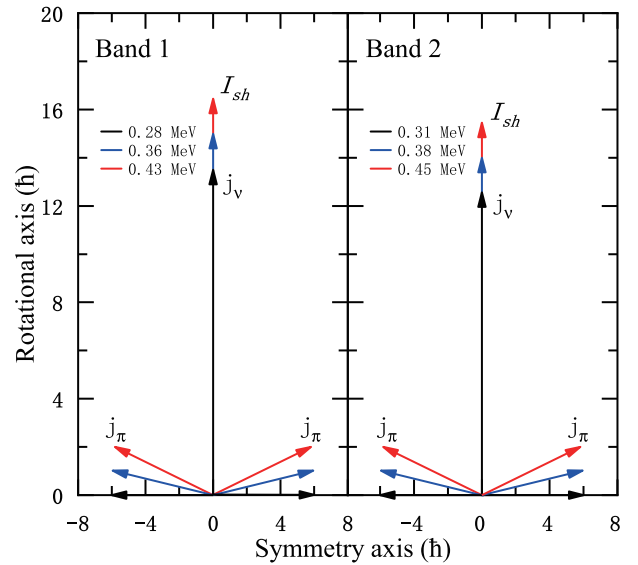**Fig. 3.** (color online) Angular momentum vectors of the two-shears-like orbits, $\boldsymbol{I}_{\mathrm{sh}}$, contributed from four proton holes $g_{9/2}^{-4}$ and neutron particles $g_{7/2}h_{11/2}^2$ for candidate AMR bands in ^{105}Pd calculated with the classical model.

Fig. 4. The value of eQ_{eff} is taken as 1.3 eb for ^{103}Pd [16] and 1.1 eb for ^{109}Cd [11]. As shown in Figs. 4(c) and (d), the $B(E2)$ values exhibit smooth decreasing tendencies with increasing rotational frequency in the calculations for all bands. However, in Figs. 4(e) and (f), the calculated $\mathfrak{I}^{(2)}/B(E2)$ ratios (>100 $\hbar^2$MeV^{-1}(eb)$^{-2}$) are significantly higher than the values for the well deformed band [9]. As mentioned above, the features of the positive-parity band in ^{103}Pd and ^{109}Cd are generally consistent with

the fingerprints of AMR. Indeed, similar to ^{105}Pd, the two-shears-like mechanism in ^{103}Pd and ^{109}Cd is clearly demonstrated in Fig. 5.

IV. SUMMARY

In this paper, the candidate multiple antimagnetic rotational bands in ^{103,105}Pd and ^{109}Cd are discussed using the classical PRM. For ^{105}Pd, the configuration of the sig-
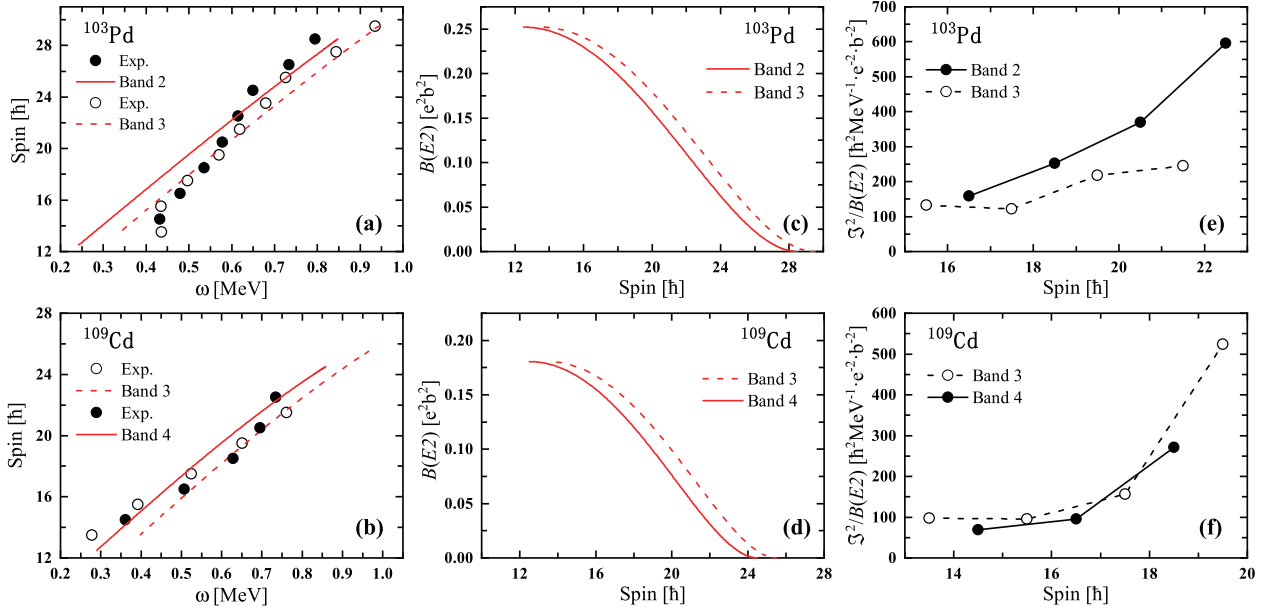

Fig. 4. (color online) Observed $I(\omega)$ plots [(a), (b)], plot of spin vs $B(E2)$ [(c), (d)], and plot of spin vs $\mathfrak{I}^{(2)}/B(E2)$ [(e), (f)] for ^{103}Pd and ^{109}Cd. The red line in (a), (b), (c), and (d) represents numerical values obtained from the classical particle-rotor model. For band 2 in ^{103}Pd, $j_\pi = 6\hbar$ and $j_\nu = 12.5\hbar$, and for band 3, $j_\nu = 13.5\hbar$. For ^{109}Cd, $j_\pi = 4.5\hbar$ and $j_\nu = 13.5\hbar$ in band 3, and $j_\nu = 12.5\hbar$ in band 4. The value of $\mathfrak{I} = 13.91$ $\hbar^2$MeV^{-1} is used for ^{103}Pd, and for ^{109}Cd, $\mathfrak{I} = 11.26$ $\hbar^2$MeV^{-1}. The $\mathfrak{I}_{rot}$ value is 18 $\hbar^2$MeV^{-1} for ^{103}Pd and 13 $\hbar^2$MeV^{-1} for ^{109}Cd.
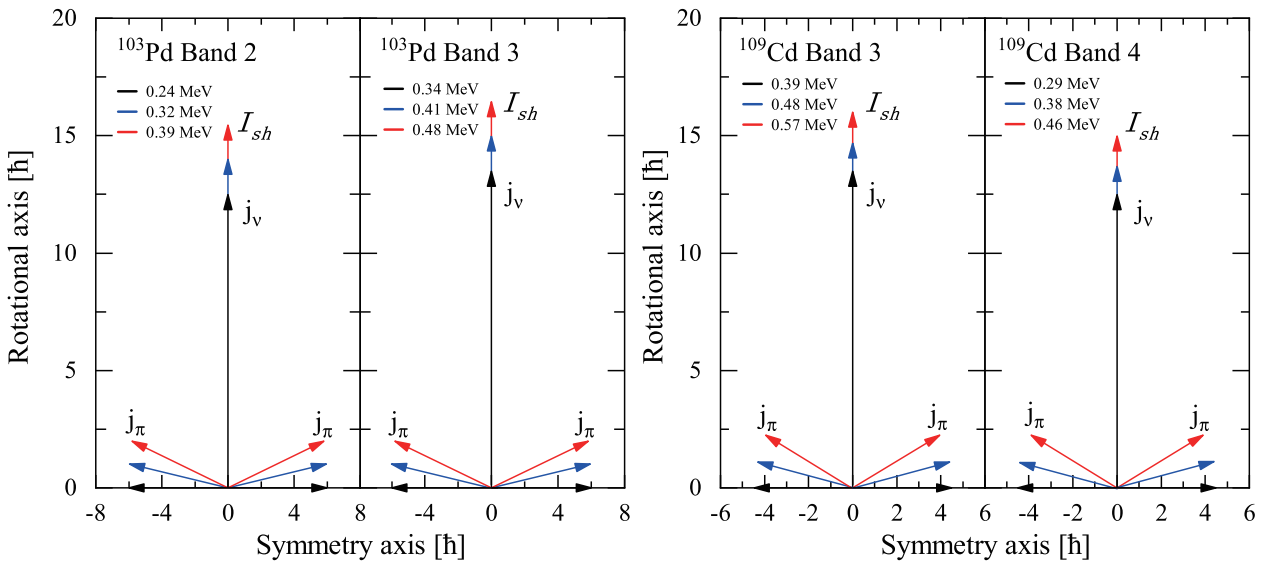

Fig. 5. (color online) Pictorial representation of the symmetric shears structure in ^{103}Pd and ^{109}Cd. The higher spin states are generated by the gradual decrease in the shears angle.

nature partner bands is assigned to $\pi(g_{9/2}^{-4}) \otimes \nu(g_{7/2} h_{11/2}^2)$, and the calculated results of the $I(\omega)$ plot further support this assignment. The calculated $B(E2)$ values show good agreement with the experimentally determined $B(E2)$ values, supporting the AMR characteristics of the signature partner bands in [105]Pd. Furthermore, the present calculations for the [103]Pd and [109]Cd nuclei predict a negative slope for the $B(E2)$ values with increasing spin and a large $\mathfrak{I}^{(2)}/B(E2)$ ratio (>100 $\hbar^2 \mathrm{MeV}^{-1}(\mathrm{eb})^{-2}$). These characteristics are consistent with the fingerprints of AMR, which suggests that the signature partner bands in [103]Pd and [109]Cd may also be candidates for AMR bands. However, to further confirm this suggestion, experimental results of the absolute $B(E2)$ transition probabilities based on lifetime measurements are desirable.

References

[1] S. Frauendorf, Nucl. Phys. A **557**, 259 (1993)
[2] S. Frauendorf, Rev. Mod. Phys. **73**, 463 (2001)
[3] S. Sihotra, D. Kumar, M. Kaur *et al.*, Phys. Rev. C **102**, 034321 (2020)
[4] D. Choudhury, A. K. Jain, M. Patial *et al.*, Phys. Rev. C **82**, 061308 (2010)
[5] A. J. Simons, R. Wadsworth, D. G. Jenkins *et al.*, Phys. Rev. Lett. **91**, 162501 (2003)
[6] A. J. Simons, R. Wadsworth, D. G. Jenkins *et al.*, Phys. Rev. C **72**, 024318 (2005)
[7] P. Datta, S. Chattopadhyay, S. Bhattacharya *et al.*, Phys. Rev. C **71**, 041305 (2005)
[8] D. Choudhury, A. K. Jain, G. Anil Kumar *et al.*, Phys. Rev. C **87**, 034304 (2013)
[9] C. Majumder, H. P. Sharma, S. Chakraborty *et al.*, Int. J. Mod. Phys. E **27**, 1850034 (2018)
[10] S. Roy, S. Chattopadhyay, P. Datta *et al.*, Phys. Lett. B **694**, 322 (2011)
[11] S. Roy and S. Chattopadhyay, Phys. Rev. C **83**, 024305 (2011)
[12] P. Zhang and B. Qi, S. Y. Wang Phys. Rev. C **89**, 047302 (2014)
[13] S. Zhu, U. Garg, A. V. Afanasjev *et al.*, Phys. Rev. C **64**, 041302 (2001)
[14] M. Sugawara, T. Hayakawa, M. Oshima *et al.*, Phys. Rev. C **92**, 024309 (2015)
[15] V. Singh, S. Sihotra, S. Roy *et al.*, J. Phys. (London) G **44**, 075105 (2017)
[16] N. Rather, S. Roy, P. Datta *et al.*, Phys. Rev. C **89**, 061303 (2014)
[17] H. Jia, B. Qi, C. Liu *et al.*, Phys. Rev. C **97**, 024335 (2018)
[18] A. Sharma, R. Raut, S. Muralithar *et al.*, Phys. Rev. C **103**, 024324 (2021)
[19] S. Ali, S. Rajbanshi, B. Das *et al.*, Phys. Rev. C **96**, 021304 (2017)
[20] S. Rajbanshi, S. Roy, S. Nag *et al.*, Phys. Lett. B **748**, 387 (2015)
[21] C. J. Chiara, D. B. Fossan, V. P. Janzen *et al.*, Phys. Rev. C **64**, 054314 (2001)
[22] M. Wang, W. J. Sun, B. H. Sun *et al.*, Eur. Phys. J. A **56**, 31 (2020)
[23] X. W. Li, J. Li, J. B. Lu *et al.*, Phys. Rev. C **86**, 057305 (2012)
[24] K. Y. Ma, J. B. Lu, J. Li *et al.*, Phys. Rev. C **100**, 014326 (2019)
[25] W. J. Sun, H. D. Xu, J. Li *et al.*, Chin. Phys. C **40**, 084101 (2016)
[26] C. Majumder, H. P. Sharma, S. S. Tiwary *et al.*, Braz. J. Phys. **49**, 539 (2019)
[27] M. Sugawara, Y. Toh, M. Oshima *et al.*, Phys. Rev. C **79**, 064321 (2009)
[28] S. Chakraborty, H. P. Sharma, S. S. Tiwary *et al.*, J. Phys. (London) G **47**, 015103 (2020)
[29] J. Peng, Int. J. Mod. Phys. E **26**, 1750051 (2017)
[30] R. M. Clark and A. O. Macchiavelli, Ann. Rev. Nucl. Part. Sci. **50**, 1 (2000)
[31] Z. H. Zhang, P. W. Zhao, J. Meng *et al.*, Phys. Rev. C **87**, 054314 (2013)
[32] Z. H. Zhang, Phys. Rev. C **94**, 034305 (2016)
[33] Z. H. Zhang, Chin. Phys. C **43**, 054107 (2019)
[34] J. Q. Ma and Z. H. Zhang, Nucl. Phys. A **1016**, 122319 (2021)
[35] S. Frauendorf, Nucl. Phys. A **677**, 115 (2000)
[36] C. J. Chiara, S. J. Asztalos, B. Busse *et al.*, Phys. Rev. C **61**, 034318 (2000)
[37] P. W. Zhao, J. Peng, H. Z. Liang *et al.*, Phys. Rev. Lett. **107**, 122501 (2011)
[38] P. W. Zhao, J. Peng, H. Z. Liang *et al.*, Phys. Rev. C **85**, 054310 (2012)
[39] L. Liu and P. W. Zhao, Sci. China Phys. Mech. Astron. **55**, 2420 (2012)
[40] J. Meng, J. Peng, S. Q. Zhang *et al.*, Front. Phys. **8**, 55 (2013)
[41] P. W. Zhao, S. Q. Zhang, and J. Meng, Phys. Rev. C **92**, 034319 (2015)
[42] P. W. Zhao, Z. P. Li, J. M. Yao *et al.*, Phys. Rev. C **82**, 054319 (2010)
[43] J. Meng and P. Zhao, Phys. Scr. **91**, 053008 (2016)
[44] P. W. Zhao, S. Q. Zhang, J. Peng *et al.*, Phys. Lett. B **699**, 181 (2011)
[45] K. Y. Ma, J. B. Lu, J. Li *et al.*, Eur. Phys. J. A **56**, 209 (2020)
[46] K. Y. Ma, J. B. Lu, D. Yang *et al.*, Eur. Phys. J. A **48**, 82 (2012)
[47] P. W. Zhao, Phys. Lett. B **773**, 1 (2017)
[48] Z. X. Ren, P. W. Zhao, and J. Meng, Phys. Rev. C **105**, L011301 (2022)
[49] P. W. Zhao, Y. K. Wang, and Q. B. Chen, Phys. Rev. C **99**, 054319 (2019)
[50] P. W. Zhao, N. Itagaki, and J. Meng, Phys. Rev. Lett. **115**, 022501 (2015)
[51] J. Meng, B. Qi, S. Q. Zhang *et al.*, Mod. Phys. Lett. A, **23**, Nos. 27, 2560 (2008)
[52] T. Koike, K. Starosta, and I. Hamamoto, Phys. Rev. Lett. **93**, 172502 (2004)
[53] B. Qi, S. Q. Zhang, J. Meng *et al.*, Phys. Lett. B **675**, 175 (2009)
[54] S. Y. Wang, S. Q. Zhang, B. Qi *et al.*, Phys. Rev. C **77**, 034314 (2008)
[55] B. G. Carlsson and I. Ragnarsson, Phys. Rev. C **74**, 044310

(2006)

[56] A. Bohr and B. Mottelson, Nuclear Structure Vol. **2**, Benjamin, New York, (1975)

[57] P. Ring and P. Shuck, Springer-Verlag, New York, (1981)

[58] J. Meng, Acta Physica Sinica **42**, 368 (1993)

[59] S. Frauendorf and J. Meng, Z. Phys. A **356**, 263 (1996)

[60] S. Frauendorf and J. Meng, Nucl. Phys. A **617**, 131 (1997)

[61] I. Ragnarsson and P. B. Semmes, Hyperfine Interactions **43**, 425 (1988)

[62] S. Q. Zhang, B. Qi, S. Y. Wang *et al*., Phys. Rev. C **75**, 044307 (2007)

[63] A. O. Macchiavelli, R. M. Clark, M. A. Deleplanque *et al*., Phys. Lett. B **450**, 1 (1999)

[64] A. O. Macchiavelli, R. M. Clark, P. Fallon *et al*., Phys. Rev. C **57**, R1073 (1998)

[65] N. Rather, P. Datta, S. Chattopadhyay *et al*., Proceedings of the DAE Symp. on Nucl. Phys. **59**, 108 (2014)

[66] S. Juutinen, P. Simecek, C. Fahlander *et al*., Nucl. Phys. A **577**, 727 (1994)

[67] B. M. Nyako, J. Gizon, A. Gizon *et al*., Phys. Rev. C **60**, 024307 (1999)